Infrared optical properties of polyaniline doped with 2-acrylamido-2-methyl-1-propanesulfonic acid (AMPSA)

2001 J. Phys.: Condens. Matter 13 6297

(http://iopscience.iop.org/0953-8984/13/29/303)

INSTITUTE OF PHYSICS PUBLISHING JOURNAL OF PHYSICS: CONDENSED MATTER

J. Phys.: Condens. Matter **13** (2001) 6297–6306 PII: S0953-8984(01)24553-6

Infrared optical properties of polyaniline doped with 2-acrylamido-2-methyl-1-propanesulfonic acid (AMPSA)

G Tzamalis[1], N A Zaidi[1], C C Homes[2] and A P Monkman[1]

[1] Department of Physics, University of Durham, South Road, Durham DH1 3LE, UK
[2] Department of Physics, Brookhaven National Laboratory, Upton, New York 11973-5000, USA

Received 3 May 2001
Published 6 July 2001
Online at stacks.iop.org/JPhysCM/13/6297

Abstract

A recent method of processing conducting polyaniline (PANi) films protonated with 2-acrylamido-2-methyl-1-propanesulfonic acid (AMPSA) and dissolved in dichloroacetic acid (DCA) has produced films of excellent stability and surface quality. We report the results of dc conductivity measurements over a wide temperature range (10–295 K) and the room temperature absolute infrared reflectivity measurements of two PANi–AMPSA films with different protonation levels. Both samples display transport properties similar to other doped conducting polymers on the metallic side of the metal–insulator transition. Further signatures of metallic behaviour can be deduced from the results of the optical measurements in the infrared range (20–8000 cm^{-1}): The samples show very high 'metal-like' reflectivity in the far infrared region, and a Drude-like behaviour, corresponding to free charge carriers, of the real part of the dielectric function for a large part of the infrared spectrum. A plasma resonance can also be observed. The localization modified Drude model is shown to fit the optical conductivity data $\sigma(\omega)$ reasonably well, supporting the notion that the new PANi–AMPSA films have the characteristics of a disordered metal on the metallic side of the metal–insulator transition.

1. Introduction

The field of conjugated polymers with intrinsically metallic behaviour has been increasingly active over the last decade and various models for interpreting the nature of the metallic state have been proposed, even though none is currently widely accepted. However, it is well established that the metallic properties of a conducting polymer depend on the doping level which is interlinked with the degree of disorder present in the sample.

Polyaniline (PANi) is an eminent member in the family of conducting polymers. It appears in three base forms: leucoemeraldine base (LB); emeraldine base (EB); and pernigraniline base (PNB) [1]. All the samples studied hereby and in the references are EB. Although insulating

in its base form, PANi displays in its doped (protonated) form (salt) transport characteristics close to the insulator–metal transition (I–M) [2, 3]. Direct current transport measurements provide information about the extent of the disorder present and identify the different transport regimes (metallic, insulating or critical) of the I–M transition. Reflectance measurements provide information about the carrier excitations and transitions over a wide energy range and can be used to determine some parameters that quantify the disorder, allowing in this way a more complete characterization of the material.

Reflectance measurements on PANi doped with camphor-sulfonic acid (CSA) have already been performed by different groups [4, 5], confirming the metal-like features and emphasizing the effect of the molecular disorder. Recently, a new acid-processing route to PANi films has been reported [6], which gives free-standing film of conspicuous stability and surface quality with room temperature dc conductivity greater than 100 S cm^{-1}, contingent on the protonation level.

In this paper the results of reflectivity measurements in the infrared range (20–8000 cm^{-1}) taken from free-standing PANi films doped with AMPSA and using dichloroacetic acid (DCA) as a solvent, are reported. Films with two different doping levels were used and the optical constants were obtained by Kramers–Kronig analysis of the reflectivity data. In conjunction with the also reported temperature dependence of the conductivity measurements, the intrinsic metallic features of PANi are once again exhibited in these films and this prompts for further structural investigation in order to reveal the role of the disorder in the transport properties of PANi.

2. Experimental procedure

2.1. Sample preparation

High molecular weight PANi ($M_w \sim 2 \times 10^5$ g mol^{-1}), synthesized in Durham at 248 K [7, 8], was used as the starting material. AMPSA and DCA were obtained from Aldrich chemicals and used without further purification or drying. Two PANi–AMPSA systems corresponding to different emeraldine base (EB)–AMPSA molar ratios were prepared for these measurements. The molar ratios used were 60% and 40% EB–AMPSA. EB PANi and AMPSA were ground in a mortar and pestle and added subsequently to DCA to obtain 2% w/w solution concentration. The solution was homogenized for about 20 min until all the lumps were dissolved, and poured onto silicon wafers in an oven at 353 K for 24 h. Two films labelled PANi–AMPSA 60% and PANi–AMPSA 40% according to their protonation levels were pealed away from the wafer and cut into thin strips. The thickness of each film was about 40–60 μm and the films were considered homogeneous and isotropic since that method of preparation does not favour any particular orientation. It must be noted that the sample preparation conditions have a strong effect to the degree of disorder present on the final sample and consequently to the observed microscopic properties [9].

2.2. Temperature dependent dc conductivity measurements

The temperature dependent conductivity measurements ranging from 10–295 K were performed inside a closed-loop helium cryostat under dynamic vacuum ($\sim 10^{-4}$ mbar). The four in-line technique was used for conductivity measurements since the samples displayed linear response in the current–voltage curve. In order to establish the best possible contacts to the sample and to minimize any contact resistance, four gold strips were evaporated on the sample surface matching spatially the contact electrodes. The sample was securely mounted

on the top of the cryostat's cold finger so that the applied pressure on the sample surface was constant and homogenous. It is assumed that in this way the contact between the electrode and the sample shows the minimum possible resistance.

2.3. Optical measurements

Normal incidence infrared reflectivity measurements in the wavenumber range 20–8000 cm^{-1} (or 0.002–0.993 eV) were taken using a Bruker IFS66v/S Fourier transform interferometer at NSLS (Beamline U10A) in Brookhaven National Laboratory. The sample was mounted as flat as possible using a thin layer of grease to adhere it in place inside the vacuum chamber, where the pressure was less than 10^{-5} mbar. Initially the reflectivity of the sample with respect to an Au reference mirror was measured. Afterwards, without altering the configuration, the chamber was connected to its built-in evaporator and gold was evaporated on the sample surface. A second reflectivity session of the gold-coated surface with respect to the same Au mirror was taken in order to account for any minor surface roughness causing light to get scattered away from the detector. In this way, the absolute reflectivity of the sample was determined by comparison of the two reflectivity spectra (after each of them was corrected using the absolute Au values from literature). During the measurements, a variety of light sources, detectors and beam splitters was used for different frequency ranges and the overlap between regions was found to be excellent.

The optical constants were calculated by Kramers–Kronig (KK) transformation of the reflectivity measurements after extrapolation to zero frequencies using the Hagen–Rubens relation $R = 1 - (2\omega/\pi\sigma_0)^{1/2}$, where σ_0 is the measured dc conductivity, and to higher frequencies using the power law ($\sim\omega^{-2}$) [10]. The KK integrals are strongly peaked at the frequency point in which they are to be determined and consequently their accurate calculation requires an adequate amount of experimental data points available in that frequency point region. The higher frequency extrapolation did not have any effect in the calculated optical constants at the low frequencies, which is the region where metallic behaviour is observed. On the other hand, the zero frequency extrapolation, being very sensitive to the dc conductivity value entered in the Hagen–Rubens formula, does not necessarily provide highly accurate data on the lower frequency region due to a limited number of experimental data points being available since measurements began at 20 cm^{-1}. Therefore, values of the optical constants at the edges of the experimentally measured region are susceptible to errors.

3. Results and discussion

3.1. Temperature dependence of dc conductivity

Figure 1 shows the $\sigma = \sigma(T)$ curves for the two PANi–AMPSA samples. The higher conductivity of the 40% (sample B) film should not strike as unusual since the optimum doping level is 50% and excess acid can inhibit the transport of the carriers. The negative temperature coefficient of conductivity, which is a fingerprint of metallic behaviour, can be observed for both samples for temperatures above 150 K. The room temperature values, the resistivity ratio $\rho(10\ \mathrm{K})/\rho(295\ \mathrm{K}) = \sigma(295\ \mathrm{K})/\sigma(10\ \mathrm{K})$ [9, 11] and the temperature of the peak conductivity values are summarized in table 1.

In both samples the resistivity ratio is less than two providing an indication that both samples are in the metallic region of the I–M transition. That samples are on the metallic side is corroborated from the activation energy plots, as shown in the inset of figure 1. The reduced activation energy $W = \mathrm{d}\ \ln\sigma/\mathrm{d}\ \ln T$ shows a positive temperature coefficient ($\mathrm{d}W/\mathrm{d}T > 0$)

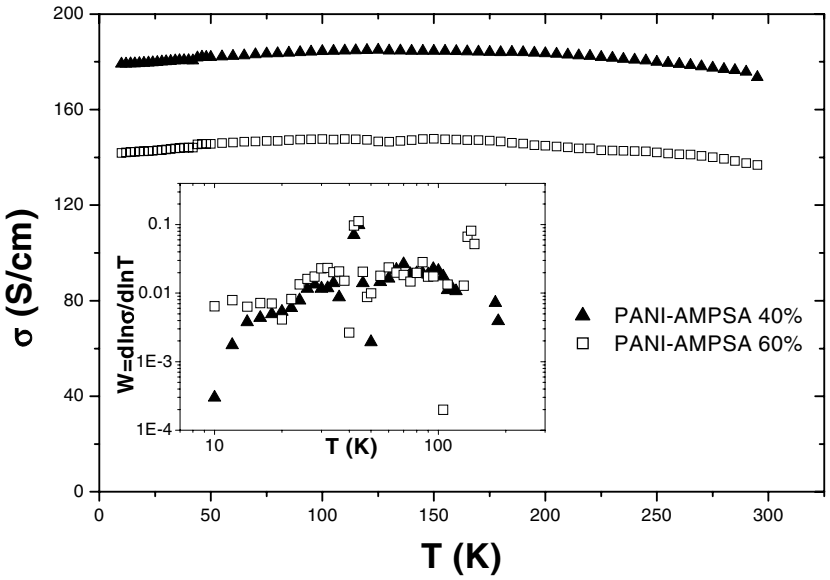

Figure 1. dc conductivity graphs as a function of temperature for PANi–AMPSA free standing films. The inset shows a log–log plot of the activation energy W against temperature.

Table 1. Values for the room temperature conductivity, the peak conductivity and its temperature and the resistivity ratio for PANi–AMPSA samples.

Sample	σ_{dc} (295 K) (S cm^{-1})	$T(\sigma_{dc}^{peak})$ (K)	σ_{dc}^{peak} (S cm^{-1})	σ(295 K)/σ (10 K)
PANi–AMPSA 60% (A)	136	150	148	0.964
PANi–AMPSA 40% (B)	173	125	185	0.969

at low temperatures for both samples with the PANi–AMPSA 40% sample having a larger slope than PANi–AMPSA 60% and therefore its metallic characteristics are more pronounced, something that is consistent with the values shown in table 1.

3.2. Optical measurements

Figure 2 shows the reflectivity spectra of the two PANi samples measured at room temperature (295 K). Similar to the previous studies of PANi–CSA [4, 12, 5], both films display very high, metal-like, reflectivity in the far infrared region (<100 cm^{-1}), where the absolute value rises above 80%. The phonon features, contrary to a metal, are not screened and are noticeable from 400–2000 cm^{-1}. After that range the curve gradually drops in a way characteristic of a semiconductor [13]. No particular features related to interband transitions are observed in that region, indicating that the onset of interband transitions occurs at higher energies. The reflectivity minimum occurs outside the measured region. Visible and ultraviolet measurements are going to follow in the future.

In order to provide further insight on the optical processes arising in the measured region, it is necessary to investigate the behaviour of the real (ε_1) and the imaginary (ε_2) part of the dielectric function ($\varepsilon = \varepsilon_1 + \mathrm{i}\varepsilon_2$) combined with the loss function Im($-\varepsilon^{-1}$) and the real part (σ) of the optical conductivity. All these quantities were calculated through Kramers–Kronig relations as described previously [10, 14], and are plotted in figures 3–5.

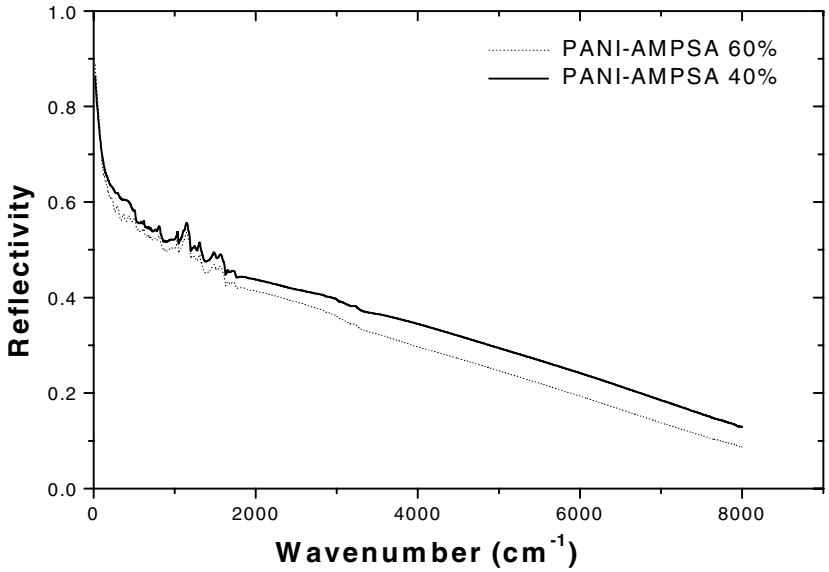

Figure 2. Room temperature reflectivity spectra of PANi–AMPSA samples from 20–8000 cm^{-1}.

Table 2. Values of the parameters derived from fitting the Drude model to the real part of the dielectric function spectrum at frequencies higher than 3000 cm^{-1}.

Sample	ε_∞	γ (cm^{-1})	ω_p (cm^{-1})
PANi–AMPSA 60% (A)	1.2	5050	8862
PANi–AMPSA 40% (B)	1.2	4806	9366

The real part of the dielectric function for both samples, although strongly screened up to 2000 cm^{-1} by the phonon features, displays behaviour resembling a Drude metal and passes through 0 at frequency Ω_p in both cases, with respective values 6344 cm^{-1} for sample A and 7155 cm^{-1} for sample B. Ω_p satisfies the plasma frequency conditions $\varepsilon_1 = 0$ and $\varepsilon_2 \ll 1$ in the vicinity of a peak in $\mathrm{Im}(-\varepsilon^{-1})$ [10, 14–16] and can therefore be identified as the screened plasma frequency of the system. It is related to the plasma frequency defined in the Drude model through the expression:

$$\Omega_p^2 = \frac{\omega_p^2}{\varepsilon_\infty} - \gamma^2$$

where $\omega_p^2 = 4\pi e^2 N/Vm^*$, the unscreened plasma frequency defined in the Drude model, N/V is the free carrier concentration, m^* is the effective mass of the charge carriers which is taken to be the free electron mass, ε_∞ is the high frequency dielectric constant and $\gamma = 1/\tau$ is the damping constant which is connected to the relaxation time τ [17]. Since the onset of the interband transitions is outside the measured region, it was sensible trying to fit the Drude expression $\varepsilon_1 = \varepsilon_\infty - \omega_p^2/(\omega^2 + \gamma^2)$ to a frequency range above that in which we observe phonon features. The fitting curved matched exactly the data curve for both cases and the results are summarized in table 2.

The above results give relaxation time $\tau \approx 10^{-15}$ s which is in agreement with past studies of PANi–CSA [12, 4, 5], and conducting polypyrrole [18–20]. For a good metal $\omega_p\tau \gg 1$ with τ varying between 10^{-13} s and 10^{-14} s. Thus, in the high frequency region fingerprints of metallic behaviour can be observed.

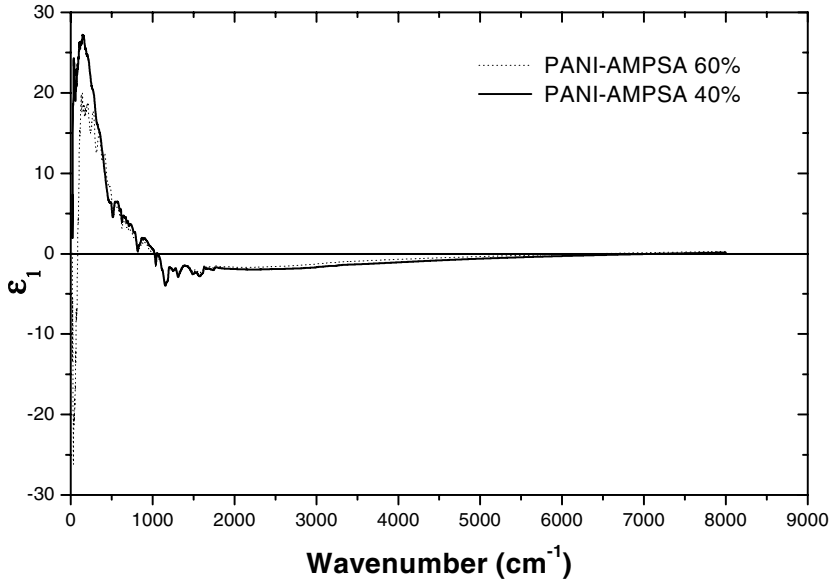

(a)

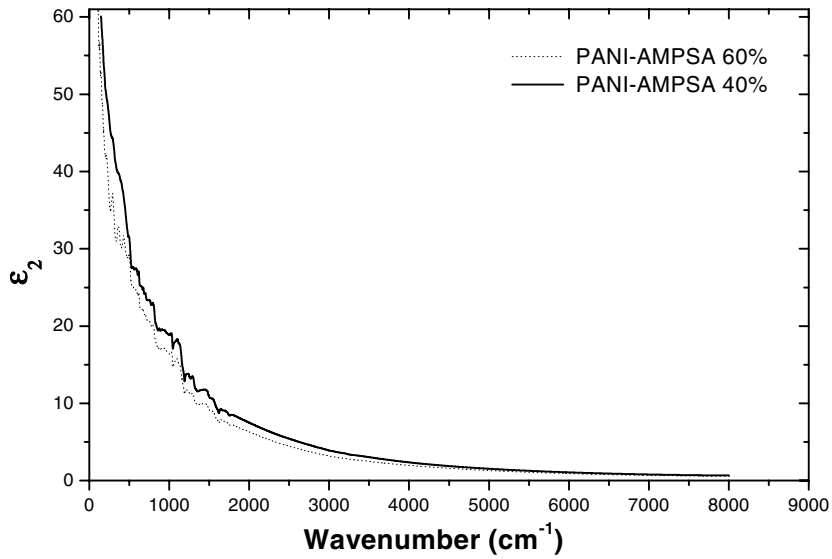

(b)

Figure 3. The real (a) and imaginary (b) parts of the dielectric function $\varepsilon = \varepsilon_1 + \mathrm{i}\varepsilon_2$ as obtained from Kramers–Kronig transformation of the reflectivity data from figure 2. The Drude model was fitted on the real part for wavenumbers greater than 3000 cm^{-1} and the results are included in table 2.

More evidence on both samples metallic behaviour can be obtained from the $\sigma(\omega)$ plots, as shown in figure 5. For ordered materials $\sigma(\omega)$ is given by the Drude formula

$$\sigma_D(\omega) = \frac{\omega_p^2 \gamma}{4\pi(\omega^2 + \gamma^2)}. \tag{1}$$

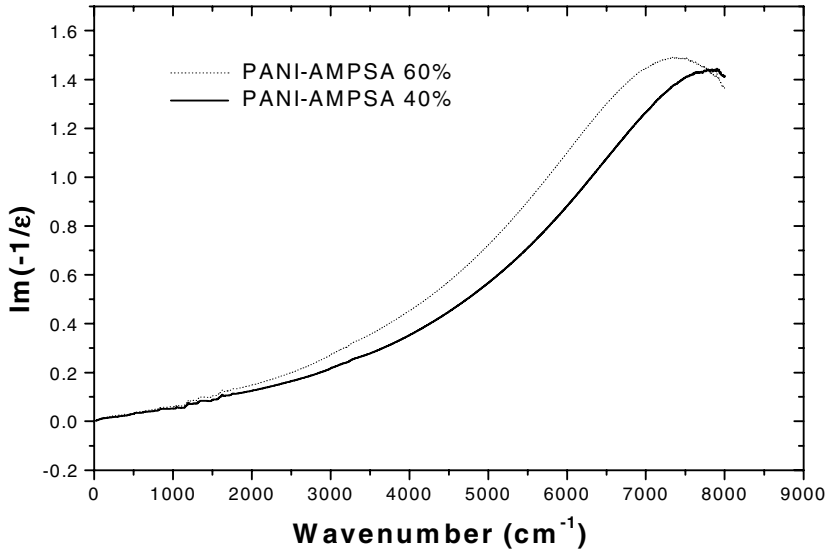

Figure 4. Graph of the energy-loss function $\mathrm{Im}(-1/\varepsilon)$. It peaks near the zero crossover of ε_1, which determines the screened plasma frequency Ω_p.

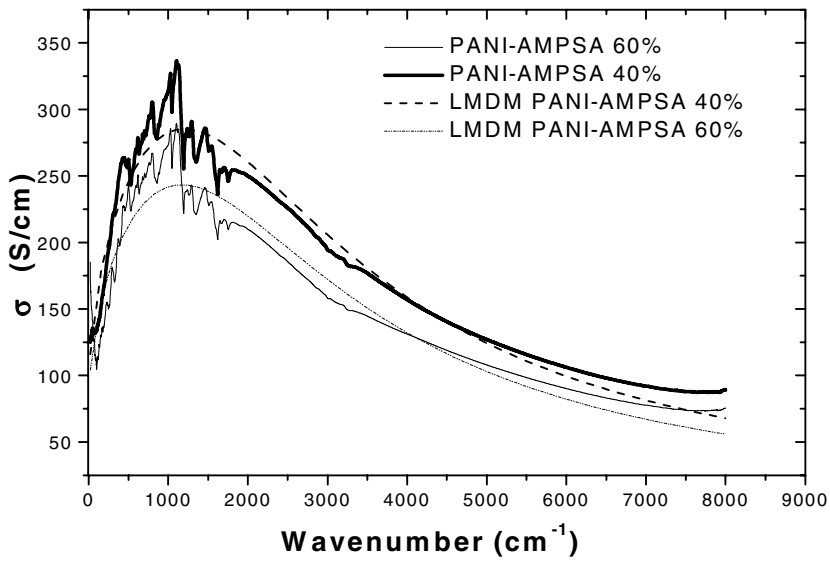

Figure 5. The optical conductivity $\sigma(\omega)$ for both samples along with the fitting curves derived from the localization modified Drude model (see equation (2)). The fitting parameters are included in table 3.

In the case of disordered material on the metallic side of the I–M transition, the scaling theories of localization have proposed, in the context of an Anderson transition, that (1) should be modified in order to account for the disorder effects which cause suppression of the conductivity at low frequencies (long-length scales) and enhancement at higher frequencies (small-length

Table 3. Values of the parameters obtained from fitting the localization modified Drude model (equation (2)) to the optical conductivity $\sigma(\omega)$ spectrum (figure 5).

Sample	$k_F\lambda$	γ (cm^{-1})	ω_p (cm^{-1})
PANi–AMPSA 60% (A)	1.18	2427	6177
PANi–AMPSA 40% (B)	1.16	2463	6725

scales). The localization modified Drude model is given by the following expression [21, 22]

$$\sigma_{LMD}(\omega) = \sigma_D(\omega)\left\{1 - \frac{C}{(k_F\lambda)^2}\left[1 - \left(\frac{3\omega}{\gamma}\right)^{1/2}\right]\right\} \tag{2}$$

where $C \approx 1$, k_F is the Fermi wavevector, and λ the mean free path. Attempts to fit (2) to the experimental data have been reasonably successful, yielding consistent values of the fitting parameters, and the results are summarized in table 3.

Although the strong phonon scattering renders an exact determination of the above parameters impossible, it is however possible to reach some qualitative conclusions about the sample properties. First, the parameter $k_F\lambda$ has been widely associated as an order parameter for the I–M transition imposing the condition $k_F\lambda > 1$ for the existence of delocalized states. The above values confirm the conclusions obtained from the previously described transport measurements regarding the metallic characteristics of both samples. Furthermore, this second set of values for γ and ω_p does not contradict the results in table 2, which were obtained from fitting the Drude model at higher frequencies, but the unscreened plasma frequency ω_p is closer to the experimental values of the screened plasma frequency Ω_p. Both sets of values suggest higher conductivity for sample B since the higher plasma frequency values lead to higher free carrier concentration values and consequently higher conductivity for similar relaxation times. The free carrier concentration values found from the plasma frequency values in table 3 are 5×10^{20} cm^{-3} for sample B and 4.2×10^{20} cm^{-3} for sample A. These values are comparable with previous results on PANi–CSA films [4, 5].

Some final remarks should be made on some features of the figures presented hereby. On the ε_1 graph (figure 3(a)), a second zero crossover at 84 cm^{-1} can be noticed in the case of sample A. In previous studies [19, 23, 24] on polypyrole, this crossover was attributed as a second plasma frequency due to a minority of delocalized carriers with unusually long scattering time ($\approx 10^{-11}$ s) and the ability to diffuse between three dimensionally ordered regions (metallic islands) without being localized. This controversial concept has been largely contested in subsequent studies on the same system [20, 3]. In the current case such an argument cannot hold since the large values of ε_2 contradict this idea. Furthermore, this behaviour is observed at the edge of the measured spectrum (20–8000) cm^{-1} and is susceptible to errors, however accurate the extrapolation technique used for the KK transformation is. Similar erratic behaviour is observed at very low frequency (<30 cm^{-1}) values of $\sigma(\omega)$ in both systems and cannot be taken into further consideration.

It is a common practice trying to relate metallic behaviour to the degree of the crystallinity present in the material. In the case of PANi–CSA films cast from m-cresol, various studies [25–27] have revealed a degree of crystallinity up to 50%, depending on the processing details. Preliminary x-ray diffraction studies on PANi–AMPSA films have failed, however, to reveal any crystallinity, despite their apparent similarity optical and transport properties to the PANi–CSA films. This may indicate that metallic behaviour in conjugated polymers does not require a large degree of crystallinity but it may instead tentatively be attributed to electron oscillations on very long conjugated segments in the polymers. Further structure studies are necessary before reaching to any conclusions regarding the correlation of metallic behaviour to sample crystallinity.

4. Conclusion

The new PANi–AMPSA system was characterized in respect to its transport and optical properties. Dc conductivity and infra-red reflectivity measurements were performed on two PANi–AMPSA samples with 60 and 40% acid doping level and in both cases the intrinsic metallic behaviour of PANi, also evident in PANi–CSA in previous sample studies, has been confirmed. In particular:

(i) Both samples display room temperature conductivity values >100 S cm^{-1} and were found to be in the metallic side of a disorder induced M–I transition, as was deduced from their resistivity ratio values and the reduced activation energy plots. The 40% sample was found more metallic than the 60%.

(ii) The infra-red optical conductivity spectra was found to fit the localization modified Drude model and the Ioffe–Regel criterion for the existence of delocalized states was satisfied since $k_F\lambda$ was found >1 for both samples. The free carrier response in the dielectric function is Drude-like for most part of the infrared spectrum. The density of free carriers was found to be in the order of 10^{20} cm^{-3} (typical value for a metal 10^{22} cm^{-3}).

The observed metallic characteristics of those two systems prompt the need for further measurements, using samples with a variety of doping levels and consequently disorder levels, so that more information about the nature of the metallic state would be available which, in combination with structure studies, could lead to a better understanding of the processes occurring in conducting polymers.

References

[1] Quillard S, Louarn G, Lefrant S and Macdiarmid A G 1994 *Phys. Rev.* B **50** 12 496
[2] Kohlman R S and Epstein A J 1998 *Handbook of Conducting Polymers* 2nd edn, ed T A Skotheim, R L Elsenbaumer and J R Reynolds (New York: Dekker)
[3] Menon R, Yoon C O, Moses D and Heeger A J 1998 *Handbook of Conducting Polymers* 2nd edn, ed T A Skotheim, R L Elsenbaumer and J R Reynolds (New York: Dekker)
[4] Lee K H, Heeger A J and Cao Y 1993 *Phys. Rev.* B **48** 14884
[5] Petit N, Gervais F, Buvat P, Hourquebie P and Topart P 1999 *Eur. Phys. J.* B **12** 367
[6] Adams P N, Devasagayam P, Pomfret S J, Abell L and Monkman A P 1998 *J. Phys.: Condens. Matter* **10** 8293
[7] Adams P N, Laughlin P J and Monkman A P 1996 *Synth. Met.* **76** 157
[8] Adams P N, Laughlin P J, Monkman A P and Kenwright A M 1996 *Polymer* **37** 3411
[9] Menon R, Yoon C O, Moses D, Heeger A J and Cao Y 1993 *Phys. Rev.* B **48** 17685
[10] Smith D Y 1998 *Handbook of Optical Constants of Solids* vol I, ed E D Palik (New York: Academic)
[11] Yoon C O, Reghu M, Moses D and Heeger A J 1994 *Phys. Rev.* B **49** 10851
[12] Lee K, Heeger A J and Cao Y 1995 *Synth. Met.* **72** 25
[13] Yu P Y and Cardona M 1996 *Fundamentals of Semiconductors* (Berlin: Springer)
[14] Wooten F 1972 *Optical Properties of Solids* (New York: Academic)
[15] Ehrenreich H and Philipp H R 1962 *Phys. Rev.* **128** 1622
[16] Cooper B R, Ehrenreich H and Philipp H R 1965 *Phys. Rev.* **138** A694
[17] Burns G 1985 *Solid State Physics* (New York: Academic)
[18] Lee K H, Menon R, Yoon C O and Heeger A J 1995 *Phys. Rev.* B **52** 4779
[19] Kohlman R S, Joo J, Wang Y Z, Pouget J P, Kaneko H, Ishiguro T and Epstein A J 1995 *Phys. Rev. Lett.* **74** 773
[20] Lee K H, Miller E K, Aleshin A N, Menon R, Heeger A J, Kim J H, Yoon C O and Lee H 1998 *Adv. Mater.* **10** 456
[21] Mott N F 1986 *Proc. 31st Scottish Universities Summer School in Physics, St Andrews* ed D M Finlayson
[22] Mott N F 1990 *Metal–Insulator Transitions* (London: Taylor and Francis)
[23] Kohlman R S, Joo J, Min Y G, MacDiarmid A G and Epstein A J 1996 *Phys. Rev. Lett.* **77** 2766
[24] Kohlman R S, Zibold A, Tanner D B, Ihas G G, Ishiguro T, Min Y G, MacDiarmid A G and Epstein A J 1997 *Phys. Rev. Lett.* **78** 3915

[25] Pouget J P, Oblakowski Z, Nogami Y, Albouy P A, Laridjani M, Oh E J, Min Y, Macdiarmid A G, Tsukamoto J, Ishiguro T and Epstein A J 1994 *Synth. Met.* **65** 131
[26] Pouget J P, Hsu C H, Macdiarmid A G and Epstein A J 1995 *Synth. Met.* **69** 119
[27] Abell L, Adams P N and Monkman A P 1996 *Polymer* **37** 5927